Highly Sensitive Coplanar Waveguide (CPW) Reflective-Mode Phase-Variation Permittivity Sensors Based on Weakly Coupled Step-Impedance Resonators (SIRs)

Pau Casacuberta, *Graduate Student Member, IEEE,* Paris Vélez, *Senior Member, IEEE,* Jonathan Muñoz-Enano, *Member, IEEE,* Lijuan Su, *Member, IEEE,* and Ferran Martín, *Fellow, IEEE*

***Abstract*—This paper presents a small-sized and highly sensitive planar microwave permittivity sensor based on a pair of weakly coupled step-impedance resonators (SIRs), the sensing elements. The sensor, a one-port structure, is implemented in coplanar waveguide (CPW) technology, and it operates in reflection mode. The sensing principle is the variation of the phase of the reflection coefficient at the operating frequency, the output variable, caused by changes in the dielectric constant of the material under test (MUT). This paper demonstrates that the maximum sensitivity is inversely proportional to the square of the electric coupling coefficient between the sensing SIRs. Thus, the sensitivity can be unprecedentedly enhanced by merely separating enough the coupled SIRs (thereby reducing their mutual coupling). Since the sensing area is circumscribed to the region occupied by the square (capacitive) patches of the SIRs, it follows that the proposed sensor exhibits also a very high figure of merit (FoM = $26551°/\lambda^2$), or ratio between the maximum sensitivity and the size of the sensing area expressed in terms of the squared guided wavelength, λ^2.**

***Index Terms*—Coplanar waveguide (CPW), coupled resonators, microwave sensor, permittivity sensor, reflective-mode sensor, step-impedance resonator (SIR).**

I. Introduction

ONE of the major challenges in the research field of planar microwave sensors is the implementation of highly sensitive devices, capable of detecting (or discriminating) small variations in the input variable, usually known as measurand. The canonical measurand in microwave sensors is the permittivity of the so-called material under test (MUT). The reason is that microwaves are highly sensitive to the dielectric properties of the medium to which they interact. Nevertheless, many other physical, chemical, and biological variables related to the permittivity, such as temperature, humidity, displacements and velocities, material composition, concentration of solute in liquid solutions, gas concentration, as well as many types of health indicators and biological analytes, can be measured by means of microwave sensors. In some cases, functional films, bio-receptors, or reagents are needed, in order to enhance the sensitivity of the device with the considered input variable.

Concerning the output variable, most planar microwave sensors reported in the literature exploit frequency variation [1]–[15]. Thus, in frequency-variation sensors, the MUT typically perturbs the capacitance of a resonant (sensing) element, resulting in a shift in the resonance frequency, the output variable. This frequency variation provides the dielectric constant of the MUT. In (non-planar) cavity sensors, the loss tangent of the MUT can also be accurately determined from the magnitude of the resonance [16]–[20]. Thus, two output variables are needed in this case, such as corresponds to the determination of two measurands, i.e., the dielectric constant and the loss tangent of the MUT (or its complex dielectric constant, with the real and the imaginary parts). Planar sensors able to provide the complex dielectric constant of the MUT have also been reported [5], [6], [14], [15] but the accuracy in the determination of the loss factor is limited, as compared to cavity sensors.

Although frequency-variation sensors are robust against the effects of noise and electromagnetic interference (EMI), such devices need wideband signals for sensing (at least covering the spectral band corresponding to the output dynamic range). This may represent an extra cost for the associated electronics in operational environments, where, rather than vector network analyzers, wideband voltage controlled oscillators (VCOs) should be used for sensor feeding (note that the generation of a sweeping signal covering a wide spectral band may represent the use of various VCOs). This bandwidth limitation applies also to the so-called frequency-splitting sensors [21]–[30], devices based on symmetry disruption caused by changes in the dielectric properties of the MUT, as compared to a reference (REF) sample. Frequency-splitting sensors are quasi-differential-mode sensors, robust against cross-sensitivities caused by variations in ambient factors (e.g., temperature and humidity) [31].

Single-frequency sensors are the solution to the previously cited bandwidth limitation. Coupling-modulation sensors [32]–[40] and phase-variation sensors [41]–[52] belong to this cate-

Manuscript received XX XXXX XXXX; revised XX XXXX XXXX; accepted XX XXXX XXXX. This work was supported by MCIN/AEI 10.13039/501100011033, Spain, through the projects PID2019-103904RB-I00, PID2022-139181OB-I00 (ERDF European Union) and PDC2021-121085-I00 (European Union Next Generation EU/PRTR), by the AGAUR Research Agency, Catalonia Government, through the project 2021-SGR00192, and by Institució Catalana de Recerca i Estudis Avançats (who awarded Ferran Martín). P. Casacuberta acknowledges the Ministerio de Universidades, Spain, for the FPU grant (Ayudas para la formación de profesorado universitario), ref. FPU20/05700. Lijuan Su acknowledges the Juan de la Cierva Program for the support through the project IJC2019-040786-I. *(Corresponding author: Pau Casacuberta.)*

The authors are with GEMMA/CIMITEC, Departament d'Enginyeria Electrònica, Universitat Autònoma de Barcelona, 08193 Bellaterra, Spain (e-mail: pau.casacuberta@uab.cat; ferran.martin@uab.es).

gory. However, phase-variation sensors combine the advantages of single-frequency operation with their intrinsic immunity to noise and EMI (by contrast, coupling modulation sensors are based on magnitude measurements, less tolerant to noise and EMI). In phase-variation sensors, the output variable is the phase of either the transmission (transmission-mode sensors [41]–[43], [50]) or the reflection (reflective-mode sensors [44]–[49], [51], [52]) coefficient. It is well known that in phase-variation sensors based on transmission lines (the sensing elements), the sensitivity, a key performance parameter, can be enhanced either by operating at high frequencies or by considering long lines (meandering has been applied in some cases) [42]. However, operating at high frequencies is not always possible, or convenient (it may increase the cost of the associated electronics), and elongating the sensing lines goes against the usual trend to reduce device dimensions as much as possible.

Recently, a novel strategy to boost up the sensitivity in one-port reflective-mode phase-variation sensors was proposed [44]. The relevant competitive advantage of such sensing approach, is that neither the operating frequency nor the length of the sensing lines should be increased. Such reflective-mode phase-variation sensors consist of a sensing element (either a distributed or a semi-lumped resonator) cascaded to a step-impedance transmission line made of high/low impedance quarter-wavelength line sections [44]–[46], [51], [52]. As it was demonstrated in [44], the sensitivity can be unprecedentedly enhanced by considering a sufficient number of high/low impedance sections exhibiting a high impedance contrast. This sensitivity enhancement is not at the expense of an increase in the sensing region, but adding (few) high/low impedance quarter-wavelength line sections is certainly required (nevertheless, it was demonstrated in [44] that with simply two line sections, sensitivities above 500° per unit of dielectric constant are achievable).

In this paper, we report a new approach for sensitivity optimization in reflective-mode phase-variation sensors. The sensing strategy, first presented in [53], also provides very high sensitivities with small sensing regions, without the need of cascading high/low impedance line sections to the sensing element. By this means, not only the area of the sensing region is kept within small values, but also the overall sensor size is reduced. Indeed, the sensing element in this novel approach is a pair of weakly coupled resonators, specifically a pair of mirrored (semi-lumped) step-impedance resonators (SIRs). Such weak coupling between the sensing SIRs is the key aspect to boost up the sensitivity, as it will be demonstrated. The sensor is implemented in coplanar waveguide (CPW) technology, more favorable to sensitivity optimization, compared to microstrip technology [53], since the MUT has a stronger effect on the variation of the capacitances of the resonant sensing elements. It should be mentioned that there are other sensors based on inter-resonator's coupling, but their principle is radically different [10], [13], [54], [55]. On the other hand, in [56], reflective-mode phase-variation sensors based on weakly coupled lines, that use a principle similar to that of the sensors presented in this paper, have been reported. The achieved sensitivities in those sensors are very competitive, but the sensing elements are distributed components (quarter-wavelength coupled lines). By contrast, the sensors presented in this work are based on semi-lumped sensing elements (a pair of weakly coupled SIRs). This contributes to reduce the size of the sensing region and to enhance the main figure of merit (FoM), defined as the ratio of the maximum sensitivity and the size of the sensing region, expressed in terms of the squared guided wavelength at the frequency of operation. Other sensors based on coupled lines have recently been proposed [57]–[61].

The organization of the paper is as follows. The sensing principle, and specifically, the strategy for sensitivity optimization based on weakly coupling the sensing resonant elements (SIRs in our case), are reported in Section II. Such section includes also the validation of the proposed circuit model of the sensor, by comparing electromagnetic simulations and circuit simulations (with extracted parameters). Section III reports a sensitivity analysis, from which it is concluded that the maximum sensitivity is inversely proportional to the square of the electric coupling coefficient between the SIRs (thereby, justifying the need for weak coupling). A prototype example is reported in Section IV, and applied to the dielectric characterization of solid samples. The effects of losses on sensitivity are studied in Section V. Section VI compares the sensor proposed in this paper with other phase-variation sensors available in the literature. Finally, Section VII summarizes the relevant aspects of the presented work.

II. Sensing principle and circuit model validation

While the reflective-mode phase-variation sensors discussed in this paper can be utilized for the measurement of various types of physical magnitudes, it is assumed herein that the input variable is the dielectric constant of the MUT, $\varepsilon_{\mathrm{MUT}}$, representing the canonical measurand. Therefore, the sensitivity is given by

$$S = \frac{d\phi_\rho}{d\varepsilon_{\mathrm{MUT}}}, \tag{1}$$

where ϕ_ρ, i.e., the output variable, is the phase of the reflection coefficient seen from the (unique) input port. From (1), it is clear that for sensitivity optimization, the maximum variation of ϕ_ρ at the (also unique) operating frequency, f_{op}, with $\varepsilon_{\mathrm{MUT}}$ must be achieved. For that purpose, the one-port sensor must exhibit a high phase slope (i.e., the slope of the phase of the reflection coefficient) with frequency at f_{op}. In these sensors, the sensitivity is not constant (sensitivity optimization is done at the expense of sensor linearity degradation). This means that it is necessary to specify the reference (REF) material, or, more specifically, the reference dielectric constant ($\varepsilon_{\mathrm{REF}}$), where the sensitivity should be optimized. Thus, for sensitivity optimization, the maximum possible phase slope with frequency at f_{op} should be achieved when the sensing element is loaded (covered) with the REF material (with dielectric constant $\varepsilon_{\mathrm{REF}}$).

A matched transmission line terminated with a resonant element, either a series or a parallel resonator, exhibits a phase slope (of the reflection coefficient) at resonance determined by the quality factor (Q-factor). Therefore, in series LC resonators, a high value of the inductance L and/or a low value of the capacitance C, providing a high Q-factor, are required in order to achieve a significant phase slope at resonance. On the contrary, the phase slope in parallel resonant tanks at resonance is

magnified by increasing C and decreasing L. This explains that in reflective-mode phase-variation sensors based on open-ended quarter-wavelength transmission line resonators (equivalent to grounded series resonator), the characteristic impedance of the line must be set to a high value (corresponding to a high Q-factor) for sensitivity optimization [44], [52]. By contrast, in sensors based on open-ended half-wavelength sensing lines (equivalent to parallel resonators), the characteristic impedance should be low (high Q-factor) [44], [51]. In practice, the Q-factor of the resonators cannot be made as high as it would be desirable. The reason is that in distributed resonators (either open-ended quarter-wavelength or open-ended half wavelength resonators) the achievable characteristic impedances of the line cannot take extreme values. In semi-lumped series resonators (such as SIRs), or parallel resonators (such as open complementary split ring resonators -OCSRRs), extreme values of the ratio L/C, as required for high Q-factors, are neither possible. For this reason, in [44], [51], [52], high/low impedance quarter-wavelength line sections have been cascaded to the sensing resonators as a means to enhance the phase slope at the operating frequency (the resonance frequency of the resonators), and consequently boost up the sensitivity.

In this paper, an alternative strategy for the design of highly sensitive reflective-mode phase-variation sensors that avoids the use of such high/low impedance quarter-wavelength line sections cascaded to the sensing element is proposed. It consists in weakly coupling a pair of identical resonators, the sensing elements, one resonator being connected to the input port of the sensor. In principle, both series and parallel coupled resonators can be considered, and their mutual coupling can be electric, magnetic, or mixed. The main idea behind this approach is that by coupling two identical resonators, a split in frequency should arise, and ideally, the phase of the reflection coefficient should undergo a 360° excursion between the two new (split) resonances, f_- and f_+. Since the separation between these two frequencies can be made arbitrarily small by weakly coupling the resonators, it follows that the phase slope at the operating frequency, f_{op}, can be made very high, provided such frequency satisfies $f_- < f_{\text{op}} < f_+$. It should be reiterated that amplifying the phase slope at f_{op} is the primary objective of this approach. By this means, it is expected that the sensitivity can be significantly enhanced (an aspect that will be demonstrated in Section III). Naturally, the presence of losses, inevitable in practice, may reduce the excursion of the phase of the reflection coefficient between f_- and f_+, but despite this restrictive aspect, the weakly-coupled-resonators' method has been found to be useful for significantly optimizing the sensitivity, as will be shown later.

Figure 1 depicts four possible sensor configurations, in which any combination of series/parallel resonators with electric/magnetic coupling is considered. In that figure, L and C are the self-inductance and self-capacitance, respectively, of the resonators, while their coupling is modeled by means of the mutual capacitance C_M (electric coupling), or the mutual inductance M (magnetic coupling). For series resonators, in the extreme case of null coupling, equivalent to an isolated resonator, the phase of the reflection coefficient at resonance, $f_{0,\text{is}}$, is $\phi_\rho = \pm 180°$ (since the input impedance is null and hence the reflection coefficient is $\rho = -1$). By coupling a resonator with the same reactive element values to the one connected to the input port (either electrically or magnetically, as depicted in the figure), the phase is $\phi_\rho = \pm 180°$ at the new resonance frequencies f_- and f_+. Therefore, the resulting phase slope between these two frequencies is significant, provided the coupling is weak (and hence f_- and f_+ are very close to each other), see Fig. 1. For parallel resonators, electrically or magnetically coupled, the phase response exhibits a null (i.e., $\phi_\rho = 0°$) at f_- and f_+, while it takes ($\phi_\rho = \pm 180°$) at the frequency f_p which is between f_- and f_+. Thus, in this case, the overall phase excursion between f_- and f_+ is also (ideally) 360°.

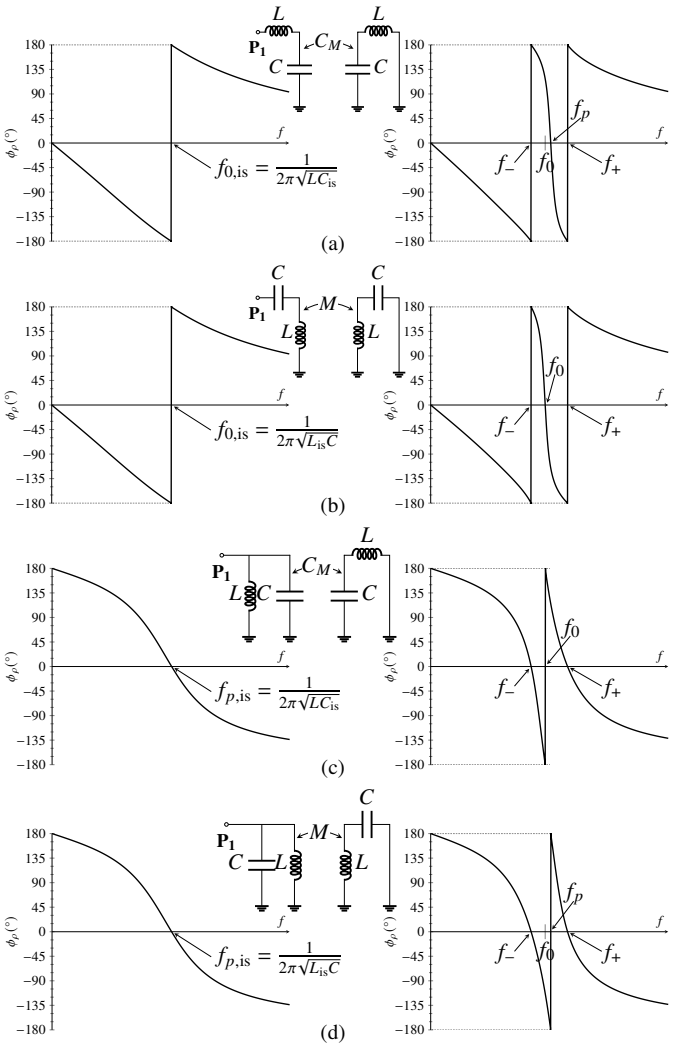

Fig. 1. Configurations of reflective-mode phase-variation sensors based on coupled resonators: (a) series resonator with electric coupling; (b) series resonator with magnetic coupling; (c) parallel resonator with electric coupling; (d) parallel resonator with magnetic coupling. The phase responses of the isolated resonators (left), as well as those corresponding to the coupled resonators (right), are also depicted.

In the present paper, the considered configuration is the one of Fig. 1(a), synthesized by means of a pair of mirrored coupled SIRs in CPW technology. A typical layout is depicted in Fig. 2. Such figure also includes the equivalent circuit model to the one depicted in Fig. 1(a). This topology takes into account the length

extension effects of the coplanar waveguide short circuit, l_{sc}, in order to maintain the same self-inductance value, L, between the left and right resonators, as presented in [62]. The input reactance of the circuit of Fig. 2(b) is

$$\chi_{in} = \frac{\left(1-k^2\right)\frac{\omega^4}{\omega_0^4} - 2\frac{\omega^2}{\omega_0^2} + 1}{C\omega\left\{\frac{\omega^2}{\omega_0^2}\left(1-k^2\right) - 1\right\}} \tag{2}$$

where ω is the angular frequency, $\omega_0 = 2\pi f_0 = 1/\sqrt{LC}$ is the angular resonance frequency of the uncoupled resonator, and $k = C_M/C$ is the electric coupling coefficient. The resonances of the coupled SIRs pair are given by those angular frequencies that nullify the reactance, namely,

$$\omega_\pm = 2\pi f_\pm = \frac{\omega_0}{\sqrt{1 \mp k}}. \tag{3}$$

It is clear, according to (3), that if the coupling is weak, then $k << 1$, and consequently, f_- and f_+ are very close one to each other. Under these conditions, as anticipated, the phase of the reflection coefficient experiences a strong variation between f_- and f_+. Thus, by tuning the operating frequency of the sensor to a value between f_- and f_+, the slope of the phase of the reflection coefficient, ϕ_ρ, with the dielectric constant of the MUT, ε_{MUT}, is expected to be high (see Section III). The procedure to determine the specific operating frequency, denoted as the optimum frequency, which should fall between the range of f_- and f_+, is outlined in Appendix A. This frequency is the one that effectively maximizes sensor sensitivity. It is pointed out in Appendix A that the optimum frequency is roughly f_p, the pole frequency, i.e., the frequency where the denominator of (2) is null, and hence $\chi_{in} = \infty$ and $\rho = 1$ (or $\phi_\rho = 0°$). The angular pole frequency is found to be

$$\omega_p = 2\pi f_p = \frac{\omega_0}{\sqrt{1-k^2}} \tag{4}$$

and the corresponding frequency, $f_p = \omega_p/2\pi$, is located slightly above f_0 and below f_+, provided the coupling is weak [see Fig. 1(a)].

For model validation, we utilized the sensing structure with dimensions as indicated in the caption of Fig. 2. The considered sensor substrate is the *Rogers 4003C* with dielectric constant $\varepsilon_r = 3.55$, thickness $h = 1.524$ mm and loss tangent $\tan\delta = 0.0021$. This structure does not take into account any REF material on top of it (it is assumed to be surrounded by air). Nevertheless, the dimensions will be redefined later to consider a specific REF material on top of the sensing region. In fact, the dimensions of the structure of Fig. 2 have been determined in order to provide a resonance frequency of the isolated resonator of $f_{0,is} = 2$ GHz. The inductance and capacitance of such isolated SIR resonator have been found to be $L = 6.54$ nH and $C_{is} = 0.97$ pF, respectively, as inferred by extracting parameters from the resonance frequency and the phase slope at resonance of the isolated SIR. Next, the mutual capacitance C_M and the self-capacitance C have been inferred from L, and the frequencies f_- and f_+ of the coupled SIRs' response. This yielded values $C = 1.006$ pF and $C_M = 0.121$ pF. The mutual coupling when air is on top of the coupled SIRs is thus $k = 0.120$. Figure 3 depicts the phase

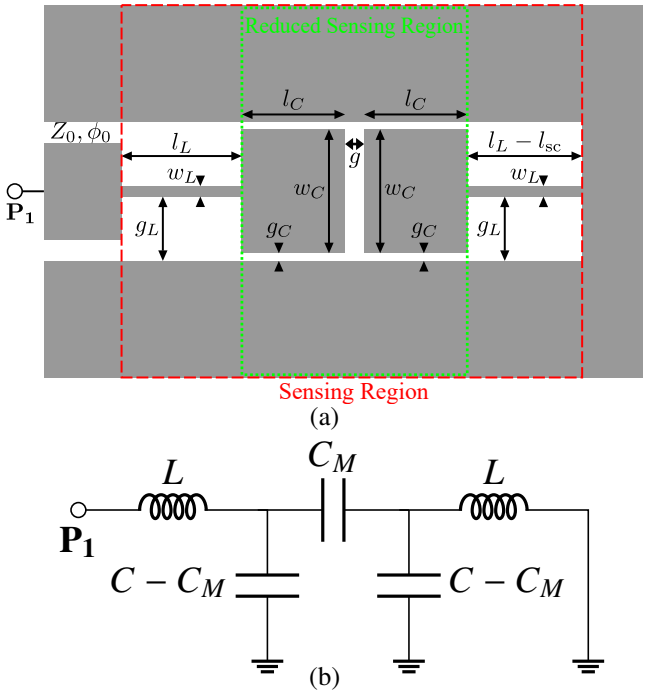

Fig. 2. Typical topology of the considered sensor (a), and circuit model that results by transforming the capacitive transformer in Fig. 1(a) to its equivalent capacitive Π-circuit (b). The sensing region is indicated with red dashes, whereas the reduced sensing region (that will be introduced in Section VI) is indicated with green dots. Dimensions (in mm) are: $l_L = 7.8$, $w_L = 0.2$, $g_L = 1.9$, $l_C = 6.37$, $w_C = 3.6$, $g_C = 0.2$, $g = 0.5$, $l_{sc} = 0.3$.

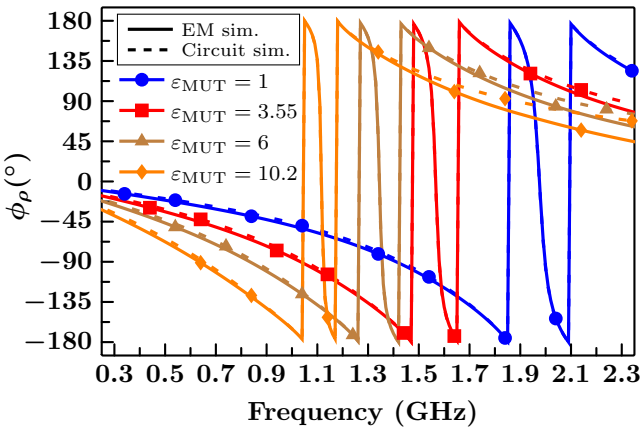

Fig. 3. Phase response of the structure of Fig. 2, with the coupled SIRs covered by air (bare SIRs) or by an MUT with the indicated dielectric constant. The circuit parameters are provided in table I.

responses inferred from circuit and electromagnetic simulations carried out using *PathWave Advanced Design System (ADS)* and *CST Microwave Studio* software, respectively. The agreement between these simulations is excellent in the region of interest. Thus, with these results, the model is validated.

III. Sensitivity Analysis

Next, an expression should be derived that provides the sensitivity as a function of the circuit and substrate parameters. In such analysis, the main hypothesis is that the electric coupling coefficient, k, does not appreciably change by varying

the dielectric constant of the material under test, $\varepsilon_{\mathrm{MUT}}$. This hypothesis is justified since the involved capacitances C and C_M are both edge capacitances, and therefore it is expected that such capacitances experience the same percentage of variation with $\varepsilon_{\mathrm{MUT}}$. In the previous section, it was considered that the REF material was air. In this section, the sensitivity analysis is generalized to encompass an arbitrary REF material, characterized by a dielectric constant $\varepsilon_{\mathrm{REF}}$. To differentiate between the capacitances C and C_M related to the coupled SIRs covered with air (bare sensor) and those when a different REF material is on top the coupled resonators, these capacitances will be redesignated as C_{REF} and $C_{M,\mathrm{REF}}$. It follows logically that if the REF material is air, then $C_{\mathrm{REF}} = C$ and $C_{M,\mathrm{REF}} = C_M$. If the REF material is semi-infinite in the vertical direction, C_{REF} and $C_{M,\mathrm{REF}}$ can be expressed in terms of C and C_M, respectively, according to [51], [52], [63]

$$C_{\mathrm{REF}} = C\frac{\varepsilon_{r,\mathrm{eq}} + \varepsilon_{\mathrm{REF}}}{\varepsilon_{r,\mathrm{eq}} + 1} \tag{5a}$$

$$C_{M,\mathrm{REF}} = C_M\frac{\varepsilon_{r,\mathrm{eq}} + \varepsilon_{\mathrm{REF}}}{\varepsilon_{r,\mathrm{eq}} + 1} \tag{5b}$$

where $\varepsilon_{r,\mathrm{eq}}$ is the equivalent dielectric constant of the substrate, defined as the dielectric constant of a hypothetical semi-infinite substrate providing the same contribution to the overall capacitance (either C_{REF} or $C_{\mathrm{M,REF}}$) [63]. The equivalent dielectric constant of the substrate depends slightly on the ratio between the gap space of the considered capacitance and the substrate thickness, and it approaches the substrate dielectric constant, ε_r, if such ratio is very small (since under these conditions the semi-infinite substrate approximation holds, and $\varepsilon_{r,\mathrm{eq}} = \varepsilon_r$). Not necessarily the equivalent dielectric constant of the substrate must be identical for both capacitances, C_{REF} and $C_{M,\mathrm{REF}}$, but the value is expected to be very similar if the gap space between both SIRs and the width of the slots between the SIR patches and the ground planes of the CPW do not differ so much. If now we designate by C' the self-capacitance of the SIRs covered with the MUT and by C'_M the mutual capacitance of the coupled SIR also covered by the MUT, it is obvious that such capacitances can be expressed as

$$C' = C_{\mathrm{REF}}\frac{\varepsilon_{r,\mathrm{eq}} + \varepsilon_{\mathrm{MUT}}}{\varepsilon_{r,\mathrm{eq}} + \varepsilon_{\mathrm{REF}}} = C\frac{\varepsilon_{r,\mathrm{eq}} + \varepsilon_{\mathrm{MUT}}}{\varepsilon_{r,\mathrm{eq}} + 1} \tag{6a}$$

$$C'_M = C_{M,\mathrm{REF}}\frac{\varepsilon_{r,\mathrm{eq}} + \varepsilon_{\mathrm{MUT}}}{\varepsilon_{r,\mathrm{eq}} + \varepsilon_{\mathrm{REF}}} = C_M\frac{\varepsilon_{r,\mathrm{eq}} + \varepsilon_{\mathrm{MUT}}}{\varepsilon_{r,\mathrm{eq}} + 1}. \tag{6b}$$

Thus, if we do assume that $\varepsilon_{r,\mathrm{eq}}$ is identical for both capacitances, as indeed it is explicitly considered in expressions (5) and (6), then it follows that k does not depend on the dielectric constant of the MUT (note that, under the considered hypothesis, $k = C_M/C = C_{M,\mathrm{REF}}/C_{\mathrm{REF}} = C'_M/C'$).

To verify the previous hypothesis (invariance of k with the material on top of the coupled SIRs), we have simulated the responses of the sensor of Fig. 2 by considering the coupled SIRs covered with different MUTs, see Fig. 3. The circuit parameters have been extracted for each case. In particular, the considered dielectric constants of the (semi-infinite) MUTs have been set to $\varepsilon_{\mathrm{MUT}} = 3.55, \varepsilon_{\mathrm{MUT}} = 6$, and $\varepsilon_{\mathrm{MUT}} = 10.2$ (nevertheless the response corresponding the higher dielectric constant is not represented in Fig. 3 to avoid an excess of curves). The inductance L does not change as compared to the one of the bare coupled SIRs, since it does not depend on the presence of a dielectric material on top of the resonators. The extracted capacitances for the different MUTs are indicated in table I, together with the resulting electric coupling coefficients. It follows from the table that the assumed hypothesis is reasonable, and hence k can be considered constant in the sensitivity analysis.

TABLE I
CAPACITANCES OF THE COUPLED SIRS FOR DIFFERENT VALUES OF THE DIELECTRIC CONSTANT OF THE MUT

	$\varepsilon_{\mathrm{MUT}}$	L (nH)	C' (pF)	C'_M (pF)	k
(air)	1	6.54	1.01	0.12	0.120
(RO4003C)	3.55	6.54	1.60	0.19	0.118
	6	6.54	2.17	0.25	0.117
(RO3010)	10.2	6.54	3.15	0.36	0.116

The sensitivity given by (1) can be expressed as follows

$$S = \frac{d\phi_\rho}{dC'} \cdot \frac{dC'}{d\varepsilon_{\mathrm{MUT}}}, \tag{7}$$

that is, a variation in the dielectric constant of the MUT, $\varepsilon_{\mathrm{MUT}}$, modifies the capacitance of the SIR, C', and it in turn perturbs the phase of the reflection coefficient, ϕ_ρ. Obviously, a change in $\varepsilon_{\mathrm{MUT}}$ has also an effect on the mutual capacitance C'_M, but the reflection coefficient, given by

$$\rho = \frac{Z_{\mathrm{in}} - Z_0}{Z_{\mathrm{in}} + Z_0} \tag{8}$$

where Z_0 is the reference impedance of the port, does not explicitly depend on C'_M, since $Z_{\mathrm{in}} = j\chi_{\mathrm{in}}$ does not either, see expression (2). The dependence of the reflection coefficient on C'_M is through k, constant as justified before. Consequently, in coherence with the considered hypothesis, expression (7) does not include a term of the form $d\phi_\rho/dC'_M \cdot dC'_M/d\varepsilon_{\mathrm{MUT}}$, as only it would be necessary if an explicit dependence of χ_{in} on C'_M was present in (2).

For the sensitivity analysis, the starting point is expression (2), where ω_0, the angular resonance frequency of the uncoupled SIR surrounded by air must be replaced with the angular resonance frequency of the uncoupled SIR covered with the MUT, ω'_0. Additionally, the self-capacitance C of the uncoupled SIR covered by air in (2) should be replaced with C'. Note that ω'_0 is simply

$$\omega'_0 = \frac{1}{\sqrt{LC'}} \tag{9}$$

and it can be expressed in terms of ω_0, or in terms of the angular resonance frequency of the SIR loaded with the REF material, $\omega_{0,\mathrm{REF}}$, in this latter case, as

$$\omega'_0 = \frac{1}{\sqrt{L\left(C_{\mathrm{REF}} + \Delta C\right)}} = \frac{\omega_{0,\mathrm{REF}}}{\sqrt{1 + \frac{\Delta C}{C_{\mathrm{REF}}}}} \tag{10}$$

where ΔC is the variation in the self-capacitance of the uncoupled SIR, with regard to the REF one, when it is loaded with the MUT (i.e., $C' = C_{\mathrm{REF}} + \Delta C$).

Moving forward, the expression (2) should be presented for the general case of the coupled SIRs loaded with an arbitrary

MUT. For that purpose, we simply need to replace ω_0 and C with ω_0' and C', respectively, in (2), i.e.,

$$\chi_{\text{in}} = \frac{\left(1-k^2\right)\frac{\omega^4}{\omega_{0,\text{REF}}^4}\left(1+\frac{\Delta C}{C_{\text{REF}}}\right)^2 - 2\frac{\omega^2}{\omega_{0,\text{REF}}^2}\left(1+\frac{\Delta C}{C_{\text{REF}}}\right)+1}{\left(C_{\text{REF}}+\Delta C\right)\omega\left\{\frac{\omega^2}{\omega_{0,\text{REF}}^2}\left(1+\frac{\Delta C}{C_{\text{REF}}}\right)\left(1-k^2\right)-1\right\}} \tag{11}$$

where expression (10) has been used. For optimal sensitivity, the operating frequency is designated as the pole frequency, $f_{p,\text{REF}}$, when the SIRs pair is loaded with the REF material (the justification is provided in Appendix A). Evaluation of the input reactance at that angular frequency, $\omega_{p,\text{REF}}$, gives

$$\chi_{\text{in}}\left(\omega_{p,\text{REF}}\right) = \frac{\frac{1}{\left(1-k^2\right)}\left(1+\frac{\Delta C}{C_{\text{REF}}}\right)^2 - 2\frac{1}{\left(1-k^2\right)}\left(1+\frac{\Delta C}{C_{\text{REF}}}\right)+1}{\left(C_{\text{REF}}+\Delta C\right)\frac{\omega_{0,\text{REF}}}{\sqrt{1-k^2}}\frac{\Delta C}{C_{\text{REF}}}} \tag{12}$$

an expression that can be simplified to

$$\chi_{\text{in}}\left(\omega_{p,\text{REF}}\right) = \frac{\frac{\Delta C^2}{C_{\text{REF}}^2}-k^2}{\left(C_{\text{REF}}+\Delta C\right)\sqrt{1-k^2}\omega_{0,\text{REF}}\frac{\Delta C}{C_{\text{REF}}}}. \tag{13}$$

Introducing (13) in (8), the reflection coefficient can be expressed as

$$\rho = \frac{jN - Z_0 D}{jN + Z_0 D}, \tag{14}$$

N and D being the numerator and the denominator, respectively, of (13), and the phase of the reflection coefficient, the relevant (output) variable, is thus

$$\phi_\rho = 2\arctan\left\{-\frac{\frac{\Delta C^2}{C_{\text{REF}}^2}-k^2}{Z_0\left(C_{\text{REF}}+\Delta C\right)\sqrt{1-k^2}\omega_{0,\text{REF}}\frac{\Delta C}{C_{\text{REF}}}}\right\}. \tag{15}$$

To compute the sensitivity, it is necessary to first derive the right-hand side of (7). After some straightforward (but tedious) calculation, the following result is obtained

$$\frac{d\phi_\rho}{d\Delta C} = -\frac{2Z_0\sqrt{1-k^2}\omega_{0,\text{REF}}\left\{\frac{\Delta C^2}{C_{\text{REF}}^2}+k^2\frac{\left(C_{\text{REF}}+2\Delta C\right)}{C_{\text{REF}}}\right\}}{Z_0^2D^2+N^2} \tag{16}$$

where it has been assumed that $d\phi_\rho/dC' = d\phi_\rho/d\Delta C$. In the limit of small variations of the dielectric constant with regard to the one of the REF material, i.e., for $C' \to C_{\text{REF}}$, or $\Delta C \to 0$, expression (16) gives

$$\left.\frac{d\phi_\rho}{d\Delta C}\right|_{\Delta C=0} = -\frac{2Z_0\omega_{0,\text{REF}}\sqrt{1-k^2}}{k^2} \equiv -\frac{2Z_0\omega_{p,\text{REF}}\left(1-k^2\right)}{k^2}. \tag{17}$$

Concerning the second term of the right-hand side member of (7), according to (6a), it is simply

$$\frac{dC'}{d\varepsilon_{\text{MUT}}} = \frac{C_{\text{REF}}}{\varepsilon_{r,\text{eq}}+\varepsilon_{\text{REF}}}. \tag{18}$$

Thus, introducing (17) and (18) in (7), the sensitivity in the limit of small perturbations for a semi-infinite MUT is found to be

$$S|_{\varepsilon_{\text{MUT}}=\varepsilon_{\text{REF}}} = -\frac{2Z_0\omega_{p,\text{REF}}\left(1-k^2\right)C_{\text{REF}}}{k^2\left(\varepsilon_{r,\text{eq}}+\varepsilon_{\text{REF}}\right)}. \tag{19}$$

From (19), it is clear that the main parameter determining the sensitivity in the limit of small perturbations is the electric coupling coefficient, k. Note that this coefficient appears squared in the denominator of (19), which means that the sensitivity in that limit can be substantially enhanced by weakly coupling the SIRs, as anticipated before. Furthermore, the term $1-k^2$ appearing in the numerator of (19) approximates to 1 when the coupling is weak. Indeed, ideally (i.e., by excluding the effects of losses, to be discussed later), the sensitivity can be boosted up to any desired value by simply reducing the electric coupling coefficient to the necessary value given by (19). In practice, a small coupling coefficient is always achievable by separating enough the SIRs. Another crucial factor impacting the sensitivity value is the dielectric constant of the substrate and reference material, represented by $\varepsilon_{r,\text{eq}}$ and ε_{REF}, respectively. These constants are vital considerations in sensor design as they appear in the denominator of (19). However, it must be taken into account that losses have been excluded in the analysis, and that their effects are expected to be more significant for high sensitivities or small coupling coefficients, this will be discussed in Section V. Moreover, by weakly coupling the resonators, tuning the operating frequency to $f_{p,\text{REF}}$ is expected to be subjected to certain difficulty, due to the proximity between f_+ and f_-. Thus, in practice, a trade off is necessary, and excessively weak coupling is not convenient. Nevertheless, as it will be shown, very high sensitivities, combined with small sensing regions, are achievable with the proposed sensing strategy, representing a very competitive approach in terms of the main Figure of Merit (FoM), or ratio between the maximum sensitivity and the area of the sensing region expressed in guided square wavelengths.

IV. Prototype Example and Experimental Validation

For validation of the proposed sensing approach, we have designed a sensor where the sensitivity has been optimized by considering that the REF material exhibits a dielectric constant of $\varepsilon_{\text{REF}} = 3.55$, the one of the *Rogers RO4003C* microwave substrate, available in our laboratory. The dimensions of the SIR have been determined so that it exhibits a pole frequency (when the sensing region is loaded with the REF material) of $f_{p,\text{REF}} = 2.003$ GHz. The device has been implemented with the same *Rogers RO4003C* substrate with dielectric constant $\varepsilon_r = 3.55$, thickness $h = 1.524$ mm and loss tangent $\tan\delta = 0.0021$ (the *LPKF H100* drilling machine has been used for that purpose). The photograph of the fabricated sensor is depicted in Fig. 4 (dimensions are indicated in the caption). The electrical parameters have been inferred from the electromagnetically simulated response by excluding losses, providing $L = 5.035$ nH, $C_{\text{REF}} = 1.276$ pF and $C_{M,\text{REF}} = 0.166$ pF (i.e., $k = 0.130$).

The simulated phase of the reflection coefficient (by including and by excluding lossess) at the pole frequency, $f_{p,\text{REF}}$, of the coupled SIRs loaded with the REF material in the sensing region, as a function of the dielectric constant of the MUT, ε_{MUT}, is depicted in Fig. 5. This figure includes also the sensitivity inferred from the derivative of the simulated data points, where it can be seen that the lossless sensitivity

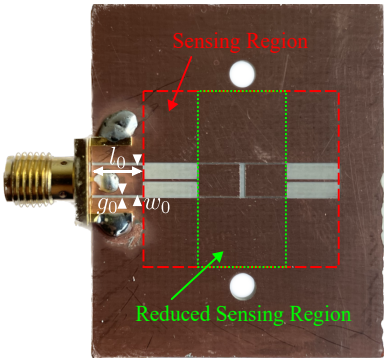

Fig. 4. Photograph of the fabricated sensor, the sensing region is indicated with red dashes, and the reduced sensing region is shown with green dots. Dimensions (in mm) are: $l_0 = 6$, $w_0 = 3.39$, $g_0 = 0.305$, $l_L = 6.40$, $w_L = 0.3$, $g_L = 1.85$, $l_C = 4.86$, $w_C = 3.6$, $g_C = 0.2$, $g = 0.62$, $l_{sc} = 0.29$.

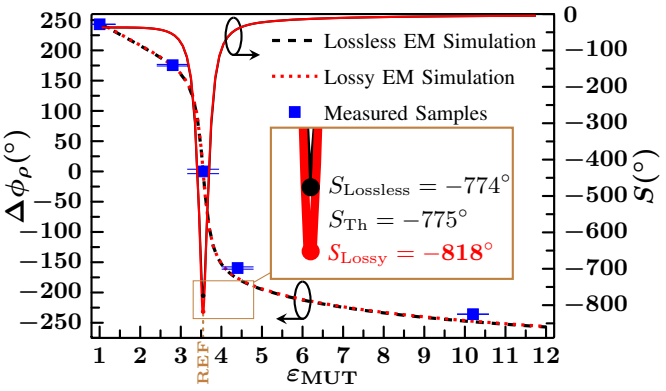

Fig. 5. Variation of the phase of the reflection coefficient at $f_{p,\text{REF}}$ as a function of ε_{MUT}, inferred from electromagnetic simulation, and sensitivity. The measured phase for the indicated MUTs is also included with error bars from a set of three independent measurements. The sensing region is the rectangle delimited by red dashes in Fig. 4.

in the limit of small perturbations, S_{Lossless}, coincides with the theoretical value, S_{Th}, given by (19), to a very good approximation. It is important to note that when losses are included, the sensitivity, S_{Lossy}, experiences a slight increment, an effect that will be discussed in Section V. It's noteworthy that the sensitivity, when including losses, has been inferred from electromagnetic simulation by considering that the loss tangent of the substrate and the one of the MUT are identical, i.e., $\tan\delta_{\text{SUB}} = \tan\delta_{\text{MUT}} = 0.0021$ (conductor losses have also been included in the lossy electromagnetic simulation). This does not represent a loss of generality, and points out that losses can help to boost up the sensitivity in the limit of small perturbations.

For evaluation of (19), the equivalent dielectric constant of the substrate, $\varepsilon_{r,\text{eq}}$, has been estimated as follows. Given a certain MUT, with a certain dielectric constant ε_{MUT} different from the one of the REF material, we have simulated the frequency response (not shown), and then we have inferred C'. Then, using (6a), $\varepsilon_{r,\text{eq}}$ can be isolated, i.e.,

$$\varepsilon_{r,\text{eq}} = \frac{\varepsilon_{\text{MUT}} C_{\text{REF}} - \varepsilon_{\text{REF}} C'}{C' - C_{\text{REF}}} \tag{20}$$

and it can be calculated since all the parameters appearing in the above expression are known. In this case, for an MUT with a dielectric constant of $\varepsilon_{\text{MUT}} = 1$, we have extracted $C' = 0.809$ pF and obtained $\varepsilon_{r,\text{eq}} = 3.36$.

Experimental validation of the fabricated sensor has been carried out by measuring the phase of the reflection coefficient at $f_{p,\text{REF}}$, for various MUTs. The measurements have been conducted utilizing a vector network analyzer, specifically the *Keysight PNA N5221A*. The MUTs are stacked slabs of uncladded microwave substrates present in our laboratory. By stacking, the semi-infinite MUT approximation is guaranteed (it has been demonstrated that a thickness of 6 mm suffices for that purpose). The measured phases, included in Fig. 5, are in good agreement with the simulated values corresponding to dielectric constants of the different samples, wich are: $\varepsilon_{\text{MUT}} = 1$ for air, $\varepsilon_{\text{MUT}} = 2.8$ for *PLA* (polylactic acid), $\varepsilon_{\text{MUT}} = 3.55$ for *Rogers RO4003C* (our reference), $\varepsilon_{\text{MUT}} = 4.4$ for *FR4*, and $\varepsilon_{\text{MUT}} = 10.2$ for *Rogers RO3010*.

In order to validate the sensor in the region of small perturbations close the REF material another type of experiment has been carried out. Specifically, we have inferred the phase of the reflection coefficient by varying the thickness of the sample under test, maintaining the dielectric constant to the one of the REF sample, i.e., 3.55. This change in the thickness translates into a variation of the equivalent dielectric constant of the MUT. This allows us to have more experimental data points for the equivalent dielectric constant of the MUT between 1 and 3.55 (or equivalently, between 0-mm and 6-mm thick MUT, the semi-infinite MUT). To be able to obtain different thickness of the MUT, we have stacked the same *RO4003C* uncladded substrate with different standard thicknesses available (0.203 mm, 0.508 mm, 0.813 mm, and 1.524 mm), abling us to provide 20 discrete values betweeen 0 mm and 6 mm. The simulated and measured points are shown in Fig. 6. Good agreement between the simulated values (considering losses) and the measured data is obtained. The insert in the figure provides the correspondence between the value of the equivalent dielectric constant, ε_{MUT}, and the thickness of the sample with a fixed $\varepsilon_{\text{MUT}} = 3.55$ (as the thickness increases, the equivalent dielectric constant tends to be 3.55, as expected). Note that for values between 2 and 6 mm the equivalent dielectric constant does not change so much. However, the phase experiences a substantial change, a consequence of the high sensitivity of the sensor.

V. Effects of Losses on the Sensitivity

This section analyzes the effects of losses on sensitivity (note that, according to Fig. 5, losses help to increase the sensitivity in the limit of small perturbations). The dielectric losses of both the MUT and substrate are modeled as conductances parallel-connected to the different capacitive elements of the model, i.e., the self-capacitance, C', and the coupling capacitance, C'_M, see Fig. 7(a). Ohmic losses, small when the metallic layer is made of a high conductive material such as Cu (with 35-μm thickness in the prototype of Fig. 4), and radiation losses, are not explicitly considered to avoid an excessively complex lossy model. Nevertheless, their potential contribution to overall losses are accounted for by the conductances that appear in Fig. 7(a) to a good approximation, as revealed by the good

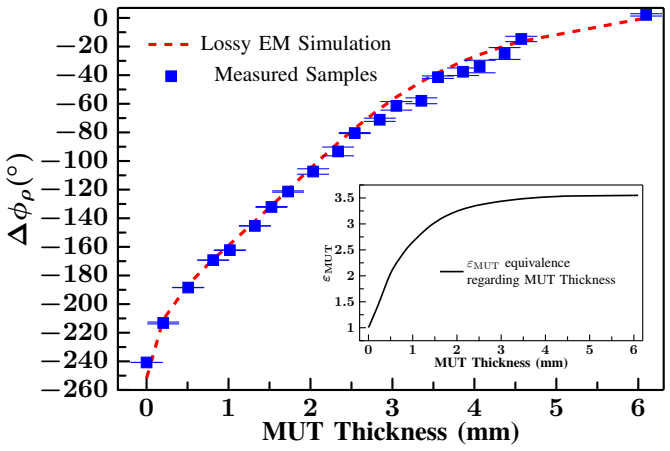

Fig. 6. Variation of the phase of the reflection coefficient at $f_{p,\mathrm{REF}}$ as a function of the thickness of the MUT sample, inferred from electromagnetic simulation. The measured phase for different values of thickness of the MUT is also included with error bars from a set of three independent measurements.

agreement between the lossy model response and the lossy electromagnetic simulations, to be demonstrated later. The link between the two conductances in the model of Fig. 7(a), through the coupling coefficient, k, is demonstrated in Appendix B.

It is important to mention that an analytical expression for the sensitivity in the limit of small perturbations with losses considered cannot be easily obtained from the model of Fig. 7(a). Nevertheless, we can compare the phase response as well as the magnitude response of the lossy electromagnetic simulation with the circuit simulation response by including losses. Very good agreement between the circuit model responses and the simulations is obtained. To validate the last statement, a set of simulations changing the value of the loss tangent ($\tan\delta_{\mathrm{MUT}}$) of the MUT has been carried out. The considered dielectric constant is the one of the REF material (repeating the simulations with other dielectric constants provides similar results but shifted in frequency, not shown). After extracting the reactive parameter values from the phase response of the reflection coefficient for a base value of losses ($\tan\delta_{\mathrm{MUT}} = 0.01$), see caption of Fig. 7, we tuned the value of G to match the same level of the magnitude of the reflection coefficient for each of the $\tan\delta_{\mathrm{MUT}}$ values reported in Fig. 7.

It can be seen from Fig. 7 that the circuit model responses are in very good agreement with the lossy EM simulations, and therefore the lossy circuit model is validated. From that premise, we can study the effects of losses on the value of the sensitivity. Obtaining two responses for close values of the dielectric constant of the MUT, $\varepsilon_{\mathrm{MUT}} = \varepsilon_{\mathrm{REF}}$ and $\varepsilon_{\mathrm{MUT}} = \varepsilon_{\mathrm{REF}} - 0.01$, and then calculating the difference of the phase response at $f_{p,\mathrm{REF}}$, we can obtain an approximation to the value of the sensitivity in the limit of small perturbations by dividing the phase difference by the variation in the permittivity (−0.01 in the considered case). Using this procedure, we can extract a set of values of sensitivity for a hypothetical reference MUT with a different value of the loss tangent while maintaining the real part of the dielectric constant. To further validate the circuit model with losses, we have also obtained the sensitivity for the values of G that make the value of the magnitude of the reflection

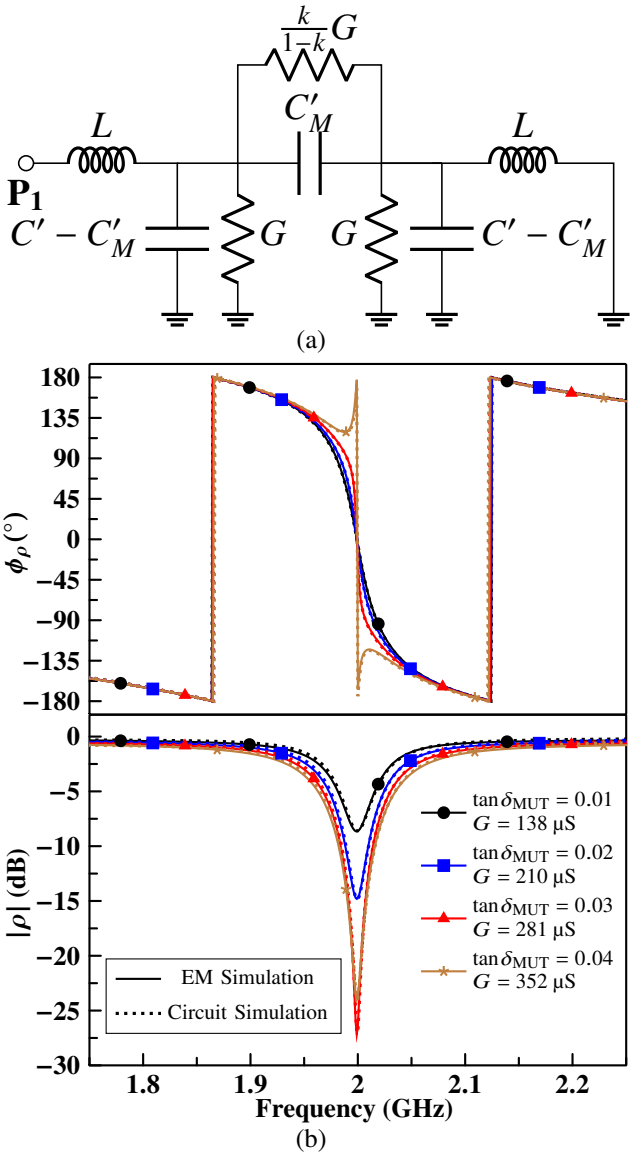

Fig. 7. Circuit model taking into account losses modeled by means of three conductances dependent on only one value of G (a) and phase and magnitude response of the reflection coefficient for different cases of loss of the MUT, for the REF case (b). The extracted reactive element values are: $C' = 1.276$ pF, $C'_M = 0.166$ pF, $L = 5.035$ nH, corresponfing to the case $\varepsilon_{\mathrm{MUT}} = \varepsilon_{\mathrm{REF}} = 3.55$.

coefficient at $f_{p,\mathrm{REF}}$ to coincide with the electromagnetic simulation taking into account all loss contributions.

One important aspect from the responses shown in Fig. 7 is that when losses increase, the phase slope at $f_{p,\mathrm{REF}}$ increases. However, there is a loss tangent of the MUT where the phase slope suddenly changes from a negative value to a positive value. When the phase slope is negative, losses are low or moderate, and this regime can be designated as low-loss regime (the analyzed case in this work). By contrast, the high-loss regime is the one where the phase slope at the operational frequency of the sensor is positive. According to these results, losses may be beneficial for sensitivity enhancement in the limit of small perturbations, because the phase slope near the frequency of operation increases with losses whilst the resonances, f_- and

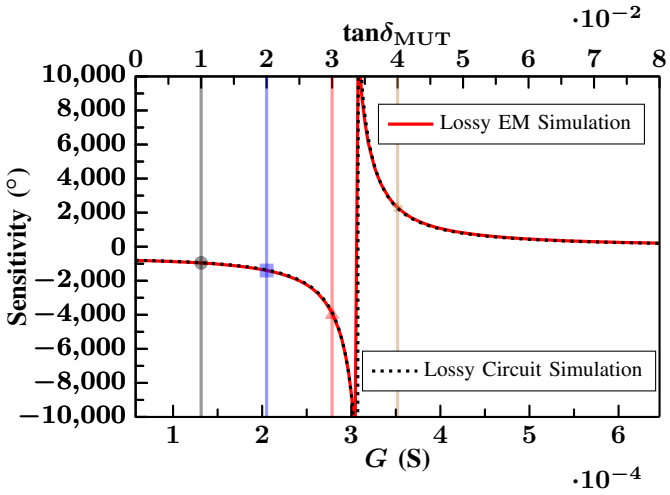

Fig. 8. Sensitivity extracted from lossy EM simulations for different values of dielectric losses in the MUT, and sensitivity extracted from the circuit model for different values of the conductance G.

TABLE II
APROXIMATED VALUES OF THE SENSITIVITY FOR DIFFERENT LEVELS OF LOSSES

$\tan\delta_{\mathrm{MUT}}$ / G	0.01 / 138 µS	0.02 / 210 µS	0.03 / 281 µS	0.04 / 352 µS
Sens. of Lossy EM sim.	−959°	−1401°	−4011°	+2338°
Sens. of Lossy Circuit sim.	−960°	−1420°	−4140°	+2256°

f_+, do not vary. Nevertheless, it should be mentioned that for a certain level of losses, the situation reverses, and the magnitude of the sensitivity decreases with losses. Such level of losses corresponds to the situation where the phase slope at $f_{p,\mathrm{REF}}$ experiences a change in its sign. Figure 8 illustrates this aspect. It can be clearly observed that the magnitude of the sensitivity first increases, it exhibits an asymptotic behavior at a particular value of the loss tangent, and then decreases. The boundary between the low-loss and the high-loss regime is thus very clear. The point at which the sensitivity exhibits an asymptotic behavior correlates to the resonators' critical coupling. In the case depicted in Fig. 8 it occurs when the loss tangent of the MUT has a value close to $\tan\delta_{\mathrm{MUT}} = 0.035$. At this point, the impedance seen from the input port matches the reference impedance, leading to complete absorption of the signal by the resonators. It is important to note, however, that operating at this critical coupling point is technically infeasible, as no signal is reflected back. Furthermore, this critical coupling point depends on various factors, including sensor properties, the characteristics of the reference MUT, the coupling level, and operating frequency.

According to Fig. 8, we can see that the sensitivity inferred from the circuit model responses exhibits a similar phenomenology to that of the EM simulation. Moreover, if we take into account the correspondence between the extracted G values and the values of $\tan\delta_{\mathrm{MUT}}$, see Fig. 7, it follows that the resulting sensitivities in the limit of small perturbations are very similar (see Fig. 8). The specific sensitivities for the loss levels of Fig. 7 are given in table II.

In summary, losses help to boost the value of the sensitivity. If the substrate and the considered MUT samples exhibit moderate or low loss tangents, the impact on sensitivity is moderate (i.e., the lossy sensitivity is slightly enhanced as compared to the lossless sensitivity), the case of the reported prototype. However, a significant improvement in the sensitivity in the limit of small perturbations is expected if losses are significant and are close to the loss level where the change of regime (from low-loss to high-loss) occurs.

VI. Comparison to Other Phase-Variation Sensors and Discussion

The sensitivity of the designed and fabricated sensor in the limit of small perturbations ($S = -818°$) is very high by virtue of the weak coupling between the sensing resonators. Taking into account the area of the sensing region, indicated in Fig. 4, the Figure of Merit is found to be FoM = $15469°/\lambda^2$, a respectable value, but not competitive if we compare it to the one in [53]. λ is the guided wavelength at the operational frequency. Nevertheless, it is worth mentioning that the overall sensor size, A_T, excluding the access line, can be considered to coincide with the size of the sensing region, A_S, indicated in Fig. 4. Note that the extra area of the fabricated sensor is irrelevant for sensing purposes, though it is necessary to position the MUT with nylon screws on top of the sensing region. The sensing region is as small as $A_S = A_T = 364\,\mathrm{mm}^2$, corresponding to $0.0529\,\lambda^2$. Such sensing region takes into account a width of 4 times the separation between the ground planes, in order to ensure that the field lines are circumscribed within the MUT. The highly achievable sensitivity (by weakly coupling the sensing resonators) and the small overall sensor size are the main competitive advantages of the proposed sensor. However, the sensing region can be significantly reduced by considering it to be delimited by the same width, but shorter length, i.e., the one corresponding to the patch capacitors, as depicted in Fig. 2 and 4. With such new sensing region, designated as reduced sensing region, the sensitivity is slightly degraded, and the new value ($S_{\mathrm{reduced}} = -620°$) deviates from the one predicted by the theory ($S_{\mathrm{Th}} = -775°$). The reason for such divergence is the fact that the narrow inductive strip of the SIR contributes to some degree to the self-capacitance, extracted by considering that the MUT covers the whole SIRs pair. However, the figure of merit with the reduced sensing region is significantly enhanced ($\mathrm{FoM}_{\mathrm{reduced}} = 26551°/\lambda^2$), which is a competitive value comparable to the one in [53], while exhibiting a higher sensitivity.

The comparative table III includes several transmission-mode and reflective-mode phase-variation sensors. Besides the FoM, as defined before, such table includes also the ratio between the maximum sensitivity and the whole device area S_{max}/A_T. As can be seen, the FoM (considering both the sensing region and the reduced sensing region) is comparable to that of other sensors reported in the available literature. However, the ratio S_{max}/A_T is by far superior in the reported device, thanks to the fact that sensitivity enhancement has been achieved without the need to cascade additional quarter-wavelength high/low impedance line sections to the sensing element, as other sensors do (e.g., [44]–[46], [51], [52]). Nevertheless, it should be noted that the

TABLE III
COMPARISON OF VARIOUS PHASE-VARIATION PERMITTIVITY SENSORS

Ref.	f_{op} (GHz)	A_S (λ^2)	A_T (λ^2)	Max. Sensitivity	FoM ($^\circ/\lambda^2$)	S_{max}/A_T ($^\circ/\lambda^2$)
[44]	2.0	0.025	0.131	528.7°	21148	4036
[45]	2.0	0.100	0.297	45.5°	455	153
[64]	2.3	—	—	600 dB	—	—
[41]	—	—	—	54.8°	—	—
[42]	6.0	12.90	12.90	415.6°	32.2	32.2
[65]	—	0.075	0.075	25.3 dB	—	—
[66]	2.0	0.020	0.400	17.6 dB	—	—
[43]	2.0	0.040	0.054	20.0°	500	370
[51]	2.0	0.015	0.073	83.35°	5643	1142
[52]	2.0	0.018	0.076	66.5°	3643	875
[53]	2.0	0.017	0.103	468°	27419	4544
[56]	2.0	0.058	0.058	736°	12690	12690
This Work	**2.0**	**0.053**	**0.053***	**818°**	**15469**	**15469**
T.W. (reduced sens. area)	**2.0**	**0.023**	**0.042***	**620°**	**26551**	**14901**

* The entries vary because the guided wavelength differs in cases where the MUT fully covers the SIR pair (extended sensing region) and when it only covers the capacitive patches (reduced sensing region). This yields a different guided wavelength for the SIRs' inductive section, leading to distinct A_T values when expressed as a function of the guided wavelength. However, the total sensor area (A_T) in cm^2 is unique and does not depend on the size of the sensing region and MUT.

sensitivity, FoM, and S/A_T in the sensors reported in [53], [56] are also very competitive. The reason is that in such sensors, boosting up the sensitivity is also based on weakly coupling a pair or resonators [53] or coupled lines [56] (i.e., additional stages are neither needed). As compared with the sensors of [53], [56], also based on weakly coupled structures, the sensor proposed in this work is implemented in CPW technology, more sensitive to variations in the dielectric constant of the MUT. In table III, the sensors reported in [64]–[66] have been included, as far as these devices are indeed sensors whose working principle is phase variation. However, phase-to-magnitude transformation is considered in such sensors, and for this reason, the sensitivity is expressed in dB, and the FoM is not given.

In summary, the use of electrically small weakly coupled resonators in the implementation of reflective-mode phase variation sensors yields highly competitive devices in terms of sensitivity, FoM, and overall sensor size.

To end this section, it should be noted that the experimental validation demonstrated in the present study has been primarily conducted using solid samples, characterized by relatively low loss and moderate values of the dielectric constant. However, this should not preclude the use of these sensors with specially designed holders or channels for analyzing the dielectric properties of liquid samples. It is crucial to emphasize that liquids typically exhibit high losses and dielectric constants. Thus, sensor sensitivity optimization by considering liquids (as MUTs) necessitates a redesign that takes into account such high losses and dielectric constants. The effects of a high dielectric constant of the MUT liquid can be compensated by reducing the coupling level, taking into consideration the effects of losses, which help to boost the sensitivity, provided the sensor is designed to operate close to the critical coupling point, as discussed before.

VII. Conclusion

In conclusion, a novel strategy for the implementation of highly sensitive reflective-mode phase-variation permittivity sensors has been proposed in this work. The sensing element is a pair of weakly coupled resonators, implemented by means of coplanar waveguide (CPW) mirrored step impedance resonators (SIRs) in this paper. It has been demonstrated that the sensitivity is inversely proportional to the square of the electric coupling coefficient between the capacitive patches of the SIRs, and this explains the potential of the approach to boost up the sensitivity (since very weak coupling can be achieved by merely separating the resonators enough). A prototype device has been designed, fabricated and experimentally characterized in order to validate the approach. As compared to other phase variation sensors, the proposed device exhibits very competitive size, performance (sensitivity) and Figure of Merit. Moreover, sensor design is very simple as far as the sensing elements are coupled SIRs, i.e., electrically small resonators well described by means of series LC tanks. An important conclusion derived from this work is that substrate and MUT losses contribute to boost up the sensitivity in the limit of small perturbations. This relevant statement has been demonstrated by comparing the sensitivity (inferred from electromagnetic simulations) with and without losses, and also from circuit simulations by including losses in the model (the good agreement with the lossy electromagnetic simulations has been instrumental to validate the model). This sensitivity enhancement related to losses is explained by the increase in the phase slope (of the reflection coefficient) at the operating frequency as the loss level increases, and is a property that other reflective-mode phase-variation sensors verify. Work is in progress to demonstrate this loss-assisted sensitivity optimization in other sensors.

Appendix A
Optimum Frequency of Operation

The purpose of this appendix is to calculate the sensitivity at any arbitrary operating frequency, and to demonstrate that the optimum frequency (the one where the sensitivity in the limit of small perturbations is maximized) is very close to $f_{p,REF}$ (the operating frequency considered in this paper). To achieve this, it is necessary to first compute the phase of the reflection coefficient. Using (11), the following result is obtained

$$\phi_\rho = 2\arctan\left\{-\frac{\left(1-k^2\right)\frac{\omega^4}{\omega_{0,\mathrm{REF}}^4}\left(1+\frac{\Delta C}{C_{\mathrm{REF}}}\right)^2-2\frac{\omega^2}{\omega_{0,\mathrm{REF}}^2}\left(1+\frac{\Delta C}{C_{\mathrm{REF}}}\right)+1}{Z_0(C_{\mathrm{REF}}+\Delta C)\,\omega\left\{\frac{\omega^2}{\omega_{0,\mathrm{REF}}^2}\left(1+\frac{\Delta C}{C_{\mathrm{REF}}}\right)\left(1-k^2\right)-1\right\}}\right\}. \tag{21}$$

From (21), and after some straightforward (but tedious) calculation, the first derivative of the right-hand side member of (7) in the limit of small perturbations ($\Delta C = 0$) is found to be

$$\left.\frac{d\phi_\rho}{d\Delta C}\right|_{\Delta C=0} = -\frac{2Z_0\omega\left\{\left(1-k^2\right)\frac{\omega^4}{\omega_{0,\mathrm{REF}}^4}-2\left(1-k^2\right)\frac{\omega^2}{\omega_{0,\mathrm{REF}}^2}+1\right\}}{Z_0^2C_{\mathrm{REF}}^2\omega^2\left\{\left(1-k^2\right)\frac{\omega^2}{\omega_{0,\mathrm{REF}}^2}-1\right\}^2+\left\{\left(1-k^2\right)\frac{\omega^4}{\omega_{0,\mathrm{REF}}^4}-2\frac{\omega^2}{\omega_{0,\mathrm{REF}}^2}+1\right\}^2}. \tag{22}$$

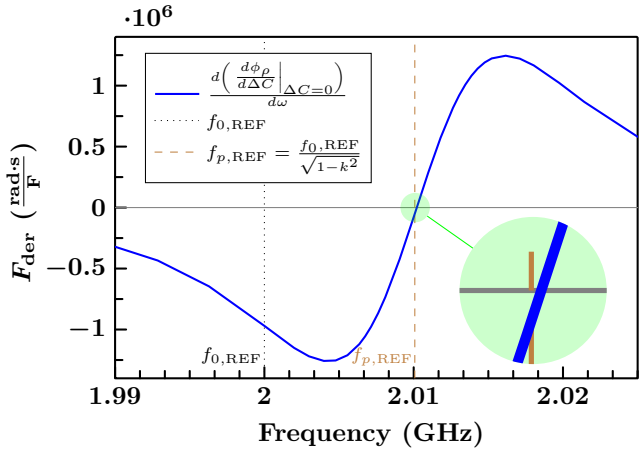

Fig. 9. Representation of expression (23), F_{der}, considering $Z_0 = 50\ \Omega$, $f_{0,\text{REF}} = 2$ GHz, $C_{\text{REF}} = 1$ pF, $k = 0.1$. The value of $f_{p,\text{REF}} = 2.01008$ GHz, indicated in the figure by the dashed line, is very close to the frequency that nulls (23), the true optimum value.

In order to determine the frequency where (22) is a maximum, it is necessary to obtain the derivative of (22) with frequency. This gives:

$$\frac{d\left(\left.\frac{d\phi_\rho}{d\Delta C}\right|_{\Delta C=0}\right)}{d\omega} = -\frac{D\cdot N' - N\cdot D'}{D^2} \equiv F_{\text{der}} \tag{23}$$

where N and D are the numerator and the denominator, respectively, of (22) and N' and D' are the corresponding derivatives, i.e.,

$$N' = 2Z_0\left\{5\left(1-k^2\right)\frac{\omega^4}{\omega_{0,\text{REF}}^4} - 6\left(1-k^2\right)\frac{\omega^2}{\omega_{0,\text{REF}}^2} + 1\right\} \tag{24}$$

$$D' = D_1' + D_2' \tag{25}$$

with

$$D_1' = 2Z_0^2C_{\text{REF}}^2\left\{\left(1-k^2\right)\frac{\omega^3}{\omega_{0,\text{REF}}^2} - \omega\right\}\left\{3\left(1-k^2\right)\frac{\omega^2}{\omega_{0,\text{REF}}^2} - 1\right\} \tag{26a}$$

$$D_2' = 2\left\{\left(1-k^2\right)\frac{\omega^4}{\omega_{0,\text{REF}}^4} - 2\frac{\omega^2}{\omega_{0,\text{REF}}^2} + 1\right\}\frac{1}{\omega}\left\{4\left(1-k^2\right)\frac{\omega^4}{\omega_{0,\text{REF}}^4} - 4\frac{\omega^2}{\omega_{0,\text{REF}}^2}\right\}. \tag{26b}$$

The optimum frequency for sensitivity optimization is found by forcing the derivative (23) to be zero. However, an analytical solution cannot be obtained. We have first checked if the optimum angular frequency is $\omega_{p,\text{REF}} = 2\pi f_{p,\text{REF}}$ by introducing this frequency in (23). The result is not null, i.e.,

$$\left.\frac{d\left(\left.\frac{d\phi_\rho}{d\Delta C}\right|_{\Delta C=0}\right)}{d\omega}\right|_{\omega_{p,\text{REF}}} = -\frac{10Z_0\left(1-k^2\right)}{k^2} \tag{27}$$

which means that, strictly speaking, the optimum frequency is not $\omega_{p,\text{REF}}$. Nevertheless, it has been found numerically that the optimum frequency is extremely close to $\omega_{p,\text{REF}}$. For that purpose, we have represented the derivative (23) for a specific case (indicated in the caption of Fig. 9) as a function of frequency, see Fig. 9, and it has been found that the optimum frequency (where (23) is null) deviates from $f_{p,\text{REF}}$ in less than 1 MHz. This is a negligible percentage of variation with regard to $f_{p,\text{REF}}$, and therefore we can assume that the optimum frequency is $f_{p,\text{REF}}$ to a very good approximation (this is the operating frequency considered in the paper). Moreover, in practice, tuning accurately the operating frequency to $f_{p,\text{REF}}$ is not exempt of certain difficulty. Actually, sensor operation at any frequency within the range comprised between f_- and f_+ is expected to provide a high sensitivity in the limit of small perturbations provided the coupling is weak (despite the fact that, certainly, the optimum frequency is, roughly, $f_{p,\text{REF}}$). For example, evaluation of (22) at $\omega_{0,\text{REF}}$ gives

$$\left.\frac{d\phi_\rho}{d\Delta C}\right|_{\Delta C=0} = -\frac{2Z_0\omega_{0,\text{REF}}}{k^2\left(1+Z_0^2\omega_{0,\text{REF}}^2C_{\text{REF}}^2\right)} \tag{28}$$

and the overall sensitivity is found to be

$$S|_{\varepsilon_{\text{MUT}}=\varepsilon_{\text{REF}}} = -\frac{2Z_0\omega_{0,\text{REF}}C_{\text{REF}}}{k^2\left(\varepsilon_{r,\text{eq}}+\varepsilon_{\text{REF}}\right)\left(1+Z_0^2\omega_{0,\text{REF}}^2C_{\text{REF}}^2\right)}. \tag{29}$$

This value is smaller than the sensitivity evaluated at $\omega_{p,\text{REF}}$ [see (19)], but note that the coupling coefficient appears squared in the denominator of (29), and hence the sensitivity can also be made high at such frequency by weakly coupling the resonators.

Appendix B
Relationship between the conductances of the lossy circuit model of the sensor

Assume that the conductance parallel connected to $C' - C'_M$ is G, whereas G_M is the conductance in parallel with C'_M, so that we must demonstrate in the present Appendix that $G_M = G\cdot k/(1-k)$, according to Fig. 7(a). To achieve this, it will be assumed that a quasi-magnetic wall exists in the slot between the SIR patches, and also in the slots between the SIR patches and the ground plane of the CPW (a reasonable hypothesis, according to [63]). Under this hypothesis, the electric field lines in such slots are roughly tangential (or parallel) to the interface between the substrate and the MUT, and both the self-capacitance C' and the mutual capacitance C'_M can be considered to be constituted by the contribution of the substrate plus the contribution of the MUT, see Fig. 10. Thus, the self-capacitance can be expressed as $C' = C'_{\text{MUT}} + C'_{\text{SUB}}$, and the mutual capacitance as $C'_M = C'_{M,\text{MUT}} + C'_{M,\text{SUB}}$. Similarly, the conductances can be expressed as the contribution of the substrate and MUT conductances, i.e., $G = G_{\text{MUT}} + G_{\text{SUB}}$, and $G_M = G_{M,\text{MUT}} + G_{M,\text{SUB}}$.

The loss tangent of the MUT can be alternatively expressed by

$$\tan\delta_{\text{MUT}} = \frac{G_{\text{MUT}}}{\omega\left(C'_{\text{MUT}} - C'_{M,\text{MUT}}\right)} \tag{30}$$

or by

$$\tan\delta_{\text{MUT}} = \frac{G_{M,\text{MUT}}}{\omega C'_{M,\text{MUT}}}, \tag{31}$$

whereas the loss tangent of the substrate is given by

$$\tan\delta_{\text{SUB}} = \frac{G_{\text{SUB}}}{\omega\left(C'_{\text{SUB}} - C'_{M,\text{SUB}}\right)} \tag{32}$$

or by

$$\tan\delta_{\text{SUB}} = \frac{G_{M,\text{SUB}}}{\omega C'_{M,\text{SUB}}}. \tag{33}$$

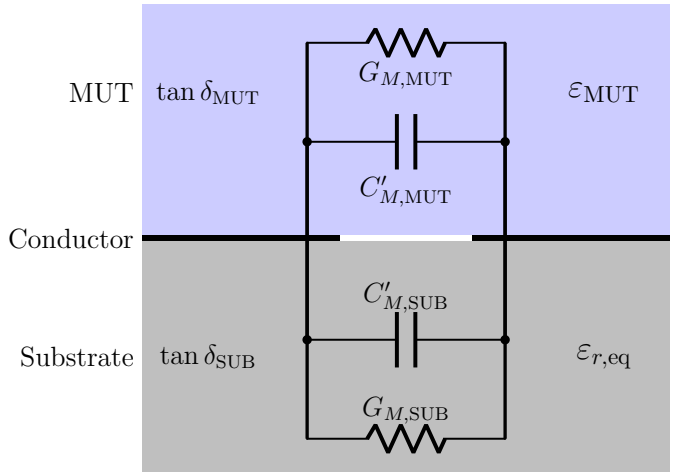

Fig. 10. Contributions of the MUT and substrate to the mutual capacitance, C'_M, and to the associated conductance, G_M. The indicated slot corresponds to the separation, g, between the SIR patches. For the parallel capacitance, $C' - C'_M$, and associated conductance, G, a similar figure applies.

Under the semi-infinite MUT approximation, it follows that the contribution of the MUT and substrate capacitances are related by

$$C'_{\mathrm{MUT}}\varepsilon_{r,\mathrm{eq}} = C'_{\mathrm{SUB}}\varepsilon_{\mathrm{MUT}} \tag{34}$$

for the self-capacitance, and by

$$C'_{M,\mathrm{MUT}}\varepsilon_{r,\mathrm{eq}} = C'_{M,\mathrm{SUB}}\varepsilon_{\mathrm{MUT}} \tag{35}$$

for the mutual capacitance. Thus, from (34) it follows that

$$C' = C'_{\mathrm{SUB}}\left(1 + \frac{\varepsilon_{\mathrm{MUT}}}{\varepsilon_{r,\mathrm{eq}}}\right) \tag{36}$$

and from (35),

$$C'_M = C'_{M,\mathrm{SUB}}\left(1 + \frac{\varepsilon_{\mathrm{MUT}}}{\varepsilon_{r,\mathrm{eq}}}\right). \tag{37}$$

Hence, it is apparent that

$$\frac{C'_M}{C'} = \frac{C'_{M,\mathrm{SUB}}}{C'_{\mathrm{SUB}}} = \frac{C'_{M,\mathrm{MUT}}}{C'_{\mathrm{MUT}}} = k. \tag{38}$$

Dividing (30) and (31), and using (38), it follows that

$$G_{M,\mathrm{MUT}} = G_{\mathrm{MUT}}\frac{k}{1-k}. \tag{39}$$

Similarly, dividing (32) and (33), one obtains

$$G_{M,\mathrm{SUB}} = G_{\mathrm{SUB}}\frac{k}{1-k} \tag{40}$$

and using

$$G_M = G_{M,\mathrm{MUT}} + G_{M,\mathrm{SUB}} \tag{41}$$

it is finally obtained

$$G_M = G_{\mathrm{MUT}}\frac{k}{1-k} + G_{\mathrm{SUB}}\frac{k}{1-k} = G\frac{k}{1-k} \tag{42}$$

in agreement with Fig. 7(a).

References

[1] A. Ebrahimi, W. Withayachumnankul, S. Al-Sarawi, and D. Abbott, "High-Sensitivity Metamaterial-Inspired Sensor for Microfluidic Dielectric Characterization," *IEEE Sensors J.*, vol. 14, no. 5, pp. 1345–1351, May 2014.

[2] M. Puentes, C. Weiß, M. Schüßler, and R. Jakoby, "Sensor array based on split ring resonators for analysis of organic tissues," in *2011 IEEE MTT-S International Microwave Symposium*, Jun. 2011, pp. 1–4.

[3] M. S. Boybay and O. M. Ramahi, "Material Characterization Using Complementary Split-Ring Resonators," *IEEE Trans. Instrum. Meas.*, vol. 61, no. 11, pp. 3039–3046, Nov. 2012.

[4] M. Schüßler, C. Mandel, M. Puentes, and R. Jakoby, "Metamaterial Inspired Microwave Sensors," *IEEE Microw. Mag.*, vol. 13, no. 2, pp. 57–68, Mar. 2012.

[5] C.-S. Lee and C.-L. Yang, "Complementary Split-Ring Resonators for Measuring Dielectric Constants and Loss Tangents," *IEEE Microw. Wirel. Compon. Lett.*, vol. 24, no. 8, pp. 563–565, Aug. 2014.

[6] C.-L. Yang, C.-S. Lee, K.-W. Chen, and K.-Z. Chen, "Noncontact Measurement of Complex Permittivity and Thickness by Using Planar Resonators," *IEEE Trans. Microw. Theory Techn.*, vol. 64, no. 1, pp. 247–257, Jan. 2016.

[7] M. Abdolrazzaghi, M. H. Zarifi, and M. Daneshmand, "Sensitivity enhancement of split ring resonator based liquid sensors," in *2016 IEEE Sens.*, Oct. 2016, pp. 1–3.

[8] L. Su, J. Mata-Contreras, P. Vélez, and F. Martín, "Estimation of the complex permittivity of liquids by means of complementary split ring resonator (CSRR) loaded transmission lines," in *2017 IEEE MTT-S International Microwave Workshop Series on Advanced Materials and Processes for RF and THz Applications (IMWS-AMP)*, Sep. 2017, pp. 1–3.

[9] L. Su, J. Mata-Contreras, P. Vélez, A. Fernández-Prieto, and F. Martín, "Analytical Method to Estimate the Complex Permittivity of Oil Samples," *Sensors*, vol. 18, no. 4, p. 984, Apr. 2018.

[10] M. Abdolrazzaghi, M. Daneshmand, and A. K. Iyer, "Strongly Enhanced Sensitivity in Planar Microwave Sensors Based on Metamaterial Coupling," *IEEE Trans. Microw. Theory Techn.*, vol. 66, no. 4, pp. 1843–1855, Apr. 2018.

[11] A. K. Jha, N. Delmonte, A. Lamecki, M. Mrozowski, and M. Bozzi, "Design of Microwave-Based Angular Displacement Sensor," *IEEE Microw. Wirel. Compon. Lett.*, vol. 29, no. 4, pp. 306–308, Apr. 2019.

[12] M. Abdolrazzaghi and M. Daneshmand, "Exploiting Sensitivity Enhancement in Micro-wave Planar Sensors Using Intermodulation Products With Phase Noise Analysis," *IEEE Trans. Circuits Syst. Regul. Pap.*, vol. 67, no. 12, pp. 4382–4395, Dec. 2020.

[13] A. M. Albishi, M. K. E. Badawe, V. Nayyeri, and O. M. Ramahi, "Enhancing the Sensitivity of Dielectric Sensors With Multiple Coupled Complementary Split-Ring Resonators," *IEEE Trans. Microw. Theory Techn.*, vol. 68, no. 10, pp. 4340–4347, Oct. 2020.

[14] A. Aquino, C. G. Juan, B. Potelon, and C. Quendo, "Dielectric Permittivity Sensor Based on Planar Open-Loop Resonator," *IEEE Sens. Lett.*, vol. 5, no. 3, pp. 1–4, Mar. 2021.

[15] J. Muñoz-Enano, P. Vélez, M. Gil, and F. Martín, "Frequency-Variation Sensors for Permittivity Measurements Based on Dumbbell-Shaped Defect Ground Structures (DB-DGS): Analytical Method and Sensitivity Analysis," *IEEE Sens. J.*, vol. 22, no. 10, pp. 9378–9386, May 2022.

[16] G. Kent, "Nondestructive permittivity measurement of substrates," *IEEE Trans. Instrum. Meas.*, vol. 45, no. 1, pp. 102–106, Feb. 1996.

[17] M. Janezic and J. Baker-Jarvis, "Full-wave analysis of a split-cylinder resonator for nondestructive permittivity measurements," *IEEE Trans. Microw. Theory Techn.*, vol. 47, no. 10, pp. 2014–2020, Oct. 1999.

[18] M. D. Janezic, "Nondestructive relative permittivity and loss tangent measurements using a split-cylinder resonator," Ph.D. dissertation, University of Colorado at Boulder, Jan. 2003.

[19] M. Janezic, E. Kuester, and J. Jarvis, "Broadband complex permittivity measurements of dielectric substrates using a split-cylinder resonator," in *2004 IEEE MTT- Int. Microw. Symp. Dig. IEEE Cat No04CH37535*, vol. 3, Jun. 2004, pp. 1817–1820 Vol.3.

[20] A. K. Jha and M. J. Akhtar, "An Improved Rectangular Cavity Approach for Measurement of Complex Permeability of Materials," *IEEE Trans. Instrum. Meas.*, vol. 64, no. 4, pp. 995–1003, Apr. 2015.

[21] P. Vélez, L. Su, K. Grenier, J. Mata-Contreras, D. Dubuc, and F. Martín, "Microwave Microfluidic Sensor Based on a Microstrip Splitter/Combiner Configuration and Split Ring Resonators (SRRs) for Dielectric Characterization of Liquids," *IEEE Sensors J.*, vol. 17, no. 20, pp. 6589–6598, Oct. 2017.

[22] A. K. Horestani, J. Naqui, Z. Shaterian, D. Abbott, C. Fumeaux, and F. Martín, "Two-dimensional alignment and displacement sensor based on movable broadside-coupled split ring resonators," *Sensors and Actuators A: Physical*, vol. 210, pp. 18–24, Apr. 2014.

[23] J. Naqui, C. Damm, A. Wiens, R. Jakoby, L. Su, and F. Martín, "Transmission lines loaded with pairs of magnetically coupled stepped impedance resonators (SIRs): Modeling and application to microwave sensors," in *2014 IEEE MTT-S International Microwave Symposium (IMS2014)*, Jun. 2014, pp. 1–4.

[24] L. Su, J. Naqui, J. Mata-Contreras, and F. Martín, "Modeling Metamaterial Transmission Lines Loaded With Pairs of Coupled Split-Ring Resonators," *IEEE Antennas Wirel. Propag. Lett.*, vol. 14, pp. 68–71, 2015.

[25] L. Su, J. Naqui, J. Mata-Contreras, and F. Martín, "Modeling and Applications of Metamaterial Transmission Lines Loaded With Pairs of Coupled Complementary Split-Ring Resonators (CSRRs)," *IEEE Antennas Wirel. Propag. Lett.*, vol. 15, pp. 154–157, 2016.

[26] J. Naqui, C. Damm, A. Wiens, R. Jakoby, L. Su, J. Mata-Contreras, and F. Martín, "Transmission Lines Loaded With Pairs of Stepped Impedance Resonators: Modeling and Application to Differential Permittivity Measurements," *IEEE Trans. Microw. Theory Techn.*, vol. 64, no. 11, pp. 3864–3877, Nov. 2016.

[27] L. Su, J. Mata-Contreras, P. Vélez, and F. Martín, "Splitter/Combiner Microstrip Sections Loaded With Pairs of Complementary Split Ring Resonators (CSRRs): Modeling and Optimization for Differential Sensing Applications," *IEEE Trans. Microw. Theory Techn.*, vol. 64, no. 12, pp. 4362–4370, Dec. 2016.

[28] A. Ebrahimi, J. Scott, and K. Ghorbani, "Differential Sensors Using Microstrip Lines Loaded With Two Split-Ring Resonators," *IEEE Sens. J.*, vol. 18, no. 14, pp. 5786–5793, Jul. 2018.

[29] A. Ebrahimi, G. Beziuk, J. Scott, and K. Ghorbani, "Microwave Differential Frequency Splitting Sensor Using Magnetic-LC Resonators," *Sensors*, vol. 20, no. 4, p. 1066, Jan. 2020.

[30] P. Vélez, F. Martín, R. Fernández-García, and I. Gil, "Embroidered Textile Frequency-Splitting Sensor Based on Stepped-Impedance Resonators," *IEEE Sens. J.*, vol. 22, no. 9, pp. 8596–8603, May 2022.

[31] F. Martín, P. Vélez, J. Muñoz-Enano, and L. Su, *Planar Microwave Sensors*, 1st ed. Wiley, Sep. 2022.

[32] J. Naqui, M. Durán-Sindreu, and F. Martín, "Novel Sensors Based on the Symmetry Properties of Split Ring Resonators (SRRs)," *Sensors*, vol. 11, no. 8, pp. 7545–7553, Aug. 2011.

[33] A. K. Horestani, C. Fumeaux, S. F. Al-Sarawi, and D. Abbott, "Displacement Sensor Based on Diamond-Shaped Tapered Split Ring Resonator," *IEEE Sensors J.*, vol. 13, no. 4, pp. 1153–1160, Apr. 2013.

[34] A. K. Horestani, D. Abbott, and C. Fumeaux, "Rotation Sensor Based on Horn-Shaped Split Ring Resonator," *IEEE Sens. J.*, vol. 13, no. 8, pp. 3014–3015, Aug. 2013.

[35] J. Naqui and F. Martín, "Transmission Lines Loaded With Bisymmetric Resonators and Their Application to Angular Displacement and Velocity Sensors," *IEEE Trans. Microw. Theory Techn.*, vol. 61, no. 12, pp. 4700–4713, Dec. 2013.

[36] J. Naqui and F. Martín, "Angular Displacement and Velocity Sensors Based on Electric-LC (ELC) Loaded Microstrip Lines," *IEEE Sensors J.*, vol. 14, no. 4, pp. 939–940, Apr. 2014.

[37] A. Horestani, J. Naqui, D. Abbott, C. Fumeaux, and F. Martín, "Two-dimensional displacement and alignment sensor based on reflection coefficients of open microstrip lines loaded with split ring resonators," *Electron. Lett.*, vol. 50, no. 8, pp. 620–622, 2014.

[38] A. Ebrahimi, W. Withayachumnankul, S. F. Al-Sarawi, and D. Abbott, "Metamaterial-Inspired Rotation Sensor With Wide Dynamic Range," *IEEE Sensors J.*, vol. 14, no. 8, pp. 2609–2614, Aug. 2014.

[39] J. Mata-Contreras, C. Herrojo, and F. Martín, "Application of Split Ring Resonator (SRR) Loaded Transmission Lines to the Design of Angular Displacement and Velocity Sensors for Space Applications," *IEEE Trans. Microw. Theory Techn.*, vol. 65, no. 11, pp. 4450–4460, Nov. 2017.

[40] J. Mata-Contreras, C. Herrojo, and F. Martín, "Detecting the Rotation Direction in Contactless Angular Velocity Sensors Implemented With Rotors Loaded With Multiple Chains of Resonators," *IEEE Sensors J.*, vol. 18, no. 17, pp. 7055–7065, Sep. 2018.

[41] F. J. Ferrández-Pastor, J. M. García-Chamizo, and M. Nieto-Hidalgo, "Electromagnetic Differential Measuring Method: Application in Microstrip Sensors Developing," *Sensors*, vol. 17, no. 7, p. 1650, Jul. 2017.

[42] J. Muñoz-Enano, P. Vélez, M. Gil Barba, and F. Martín, "An Analytical Method to Implement High-Sensitivity Transmission Line Differential Sensors for Dielectric Constant Measurements," *IEEE Sens. J.*, vol. 20, no. 1, pp. 178–184, Jan. 2020.

[43] A. Ebrahimi, J. Coromina, J. Muñoz-Enano, P. Vélez, J. Scott, K. Ghorbani, and F. Martín, "Highly Sensitive Phase-Variation Dielectric Constant Sensor Based on a Capacitively-Loaded Slow-Wave Transmission Line," *IEEE Trans. Circuits Syst. Regul. Pap.*, vol. 68, no. 7, pp. 2787–2799, Jul. 2021.

[44] J. Muñoz-Enano, P. Vélez, L. Su, M. Gil, P. Casacuberta, and F. Martín, "On the Sensitivity of Reflective-Mode Phase-Variation Sensors Based on Open-Ended Stepped-Impedance Transmission Lines: Theoretical Analysis and Experimental Validation," *IEEE Trans. Microw. Theory Techn.*, vol. 69, no. 1, pp. 308–324, Jan. 2021.

[45] L. Su, J. Muñoz-Enano, P. Velez, P. Casacuberta, M. Gil, and F. Martín, "Highly Sensitive Phase Variation Sensors Based on Step-Impedance Coplanar Waveguide (CPW) Transmission Lines," *IEEE Sens. J.*, vol. 21, no. 3, pp. 2864–2872, Feb. 2021.

[46] P. Casacuberta, J. Muñoz-Enano, P. Vélez, L. Su, M. Gil, and F. Martín, "Highly Sensitive Reflective-Mode Defect Detectors and Dielectric Constant Sensors Based on Open-Ended Stepped-Impedance Transmission Lines," *Sensors*, vol. 20, no. 21, p. 6236, Jan. 2020.

[47] A. K. Jha, A. Lamecki, M. Mrozowski, and M. Bozzi, "A Highly Sensitive Planar Microwave Sensor for Detecting Direction and Angle of Rotation," *IEEE Trans. Microw. Theory Techn.*, vol. 68, no. 4, pp. 1598–1609, Apr. 2020.

[48] A. K. Horestani, Z. Shaterian, and F. Martín, "Rotation Sensor Based on the Cross-Polarized Excitation of Split Ring Resonators (SRRs)," *IEEE Sens. J.*, vol. 20, no. 17, pp. 9706–9714, Sep. 2020.

[49] J. Muñoz-Enano, P. Vélez, L. Su, M. Gil-Barba, and F. Martín, "A Reflective-Mode Phase-Variation Displacement Sensor," *IEEE Access*, vol. 8, pp. 189 565–189 575, 2020.

[50] L. Su, J. Muñoz-Enano, P. Vélez, P. Casacuberta, M. Gil, and F. Martín, "Phase-Variation Microwave Sensor for Permittivity Measurements Based on a High-Impedance Half-Wavelength Transmission Line," *IEEE Sensors J.*, vol. 21, no. 9, pp. 10 647–10 656, May 2021.

[51] L. Su, J. Muñoz-Enano, P. Vélez, M. Gil-Barba, P. Casacuberta, and F. Martín, "Highly Sensitive Reflective-Mode Phase-Variation Permittivity Sensor Based on a Coplanar Waveguide Terminated With an Open Complementary Split Ring Resonator (OCSRR)," *IEEE Access*, vol. 9, pp. 27 928–27 944, 2021.

[52] P. Casacuberta, P. Vélez, J. Muñoz-Enano, L. Su, M. G. Barba, A. Ebrahimi, and F. Martín, "Circuit Analysis of a Coplanar Waveguide (CPW) Terminated With a Step-Impedance Resonator (SIR) for Highly Sensitive One-Port Permittivity Sensing," *IEEE Access*, vol. 10, pp. 62 597–62 612, 2022.

[53] P. Casacuberta, P. Vélez, J. Muñoz-Enano, L. Su, M. Gil, and F. Martín, "Reflective-Mode Phase-Variation Permittivity Sensors Based on Coupled Resonators," in *2022 IEEE Sens.*, Oct. 2022, pp. 1–4.

[54] C. G. Juan, B. Potelon, C. Quendo, E. Bronchalo, and J. M. Sabater-Navarro, "Highly-Sensitive Glucose Concentration Sensor Exploiting Inter-resonators Couplings," in *2019 49th Eur. Microw. Conf. (EuMC)*, Oct. 2019, pp. 662–665.

[55] Z. Xu, Y. Wang, and S. Fang, "Dielectric Characterization of Liquid Mixtures Using EIT-like Transmission Window," *IEEE Sens. J.*, vol. 21, no. 16, pp. 17 859–17 867, Aug. 2021.

[56] P. Casacuberta, P. Vélez, J. Muñoz-Enano, L. Su, and F. Martín, "Highly Sensitive Reflective-Mode Phase-Variation Permittivity Sensors Using Coupled Line Sections," *IEEE Trans. Microw. Theory Techn.*, vol. 71, pp. 2970–2984, July 2023.

[57] I. Piekarz, J. Sorocki, K. Wincza, and S. Gruszczynski, "Microwave Sensors for Dielectric Sample Measurement Based on Coupled-Line Section," *IEEE Trans. Microw. Theory Techn.*, vol. 65, no. 5, pp. 1615–1631, May 2017.

[58] J. Sorocki, I. Piekarz, K. Wincza, S. Gruszczynski, and J. Papapolymerou, "Broadband Microwave Microfluidic Coupled-Line Sensor With 3-D-Printed Channel for Industrial Applications," *IEEE Trans. Microw. Theory Techn.*, vol. 68, no. 7, pp. 2808–2822, Jul. 2020.

[59] I. Piekarz, J. Sorocki, K. Wincza, and S. Gruszczynski, "Coupled-Line Sensor With Marchand Balun as RF System for Dielectric Sample Detection," *IEEE Sensors J.*, vol. 16, no. 1, pp. 88–96, Jan. 2016.

[60] Z. R. Omam, V. Nayyeri, and O. M. Ramahi, "Microstrip Coupled-Line Directional Coupler for High-Sensitivity Dielectric Constant Measurement," in *2021 51st Eur. Microw. Conf. (EuMC)*, Apr. 2022, pp. 413–416.

[61] Z. R. Omam, V. Nayyeri, S.-H. Javid-Hosseini, and O. M. Ramahi, "Simple and High-Sensitivity Dielectric Constant Measurement Using a High-Directivity Microstrip Coupled-Line Directional Coupler," *IEEE Trans. Microw. Theory Techn.*, vol. 70, no. 8, pp. 3933–3942, Aug. 2022.

[62] R. Simons, *Coplanar Waveguide Discontinuities and Circuit Elements*, ser. Wiley Series in Microwave and Optical Engineering. New York: John Wiley, 2001, pp. 237–287.

[63] J. Muñoz-Enano, J. Martel, P. Vélez, F. Medina, L. Su, and F. Martín, "Parametric Analysis of the Edge Capacitance of Uniform Slots and

Application to Frequency-Variation Permittivity Sensors," *Appl. Sci.*, vol. 11, no. 15, p. 7000, Jul. 2021.
[64] C. Damm, M. Schüßler, M. Puentes, H. Maune, M. Maasch, and R. Jakoby, "Artificial transmission lines for high sensitive microwave sensors," in *2009 IEEE Sens.*, Oct. 2009, pp. 755–758.
[65] M. Gil, P. Vélez, F. Aznar-Ballesta, J. Muñoz-Enano, and F. Martín, "Differential Sensor Based on Electroinductive Wave Transmission Lines for Dielectric Constant Measurements and Defect Detection," *IEEE Trans. Antennas Propag.*, vol. 68, no. 3, pp. 1876–1886, Mar. 2020.
[66] J. Muñoz-Enano, P. Vélez, M. Gil Barba, J. Mata-Contreras, and F. Martín, "Differential-Mode to Common-Mode Conversion Detector Based on Rat-Race Hybrid Couplers: Analysis and Application to Differential Sensors and Comparators," *IEEE Trans. Microw. Theory Techn.*, vol. 68, no. 4, pp. 1312–1325, Apr. 2020.

Pau Casacuberta (GS'22) was born in Sabadell (Barcelona), Spain, in 1997. He received the Bachelor's Degree in Electronic Telecommunications Engineering and Computer Engineering from the Universitat Autònoma de Barcelona (UAB) in 2020, and the master's degree in Telecommunications Engineering in 2022. He received the Collaboration fellowship by the Spanish Government in 2019 for developing his Bachelor's Thesis in highly sensitive microwave sensors based in stepped impedance structures. Furthermore, he is currently working in the elaboration of his PhD, which is focused on the development of microwave sensors for the characterization of the composition of multicomponent liquid substances, with a research grant from FPU Program of the Universities Spanish Ministry.

Paris Vélez (S'10–M'14–SM'21) was born in Barcelona, Spain, in 1982. He received the degree in Telecommunications Engineering, specializing in electronics, the Electronics Engineering degree, and the Ph.D. degree in Electrical Engineering from the Universitat Autònoma de Barcelona, Spain, in 2008, 2010, and 2014, respectively. His Ph.D. thesis concerned common mode suppression differential microwave circuits based on metamaterial concepts and semi-lumped resonators. During the Ph.D., he was awarded with a pre-doctoral teaching and research fellowship by the Spanish Government from 2011 to 2014. From 2015-2017, he was involved in the subjects related to metamaterials sensors for fluidics detection and characterization at LAAS-CNRS through a TECNIOSpring fellowship cofounded by the Marie Curie program. From 2018 to 2020 he has worked in miniaturization of passive circuits RF/microwave and sensors-based metamaterials through Juan de la Cierva fellowship. His current research interests include the miniaturization of passive circuits RF/microwave and sensors-based metamaterials. Dr. Vélez is a Reviewer for the IEEE Transactions on Microwave Theory and Techniques and for other journals.

Jonathan Muñoz-Enano (S'19) was born in Mollet del Vallès (Barcelona), Spain, in 1994. He received the Bachelor's Degree in Electronic Telecommunications Engineering in 2016 and the Master's Degree in Telecommunications Engineering in 2018, both at the Autonomous University of Barcelona (UAB). Actually, he is working in the same university in the elaboration of his PhD, which is focused on the development of microwave sensors based on metamaterials concepts for the dielectric characterization of materials and biosensors.

Lijuan Su was born in Qianjiang (Hubei), China in 1983. She received the B.S. degree in communication engineering and the M.S. degree in circuits and systems both from Wuhan University of Technology, Wuhan, China, in 2005 and 2013 respectively, and the Ph.D. degree in electronic engineering from Universitat Autònoma de Barcelona, Barcelona, Spain, in 2017. From Nov. 2017 to Dec. 2019, she worked as a postdoc researcher in Flexible Electronics Research Center, Huazhong University of Science and Technology, Wuhan, China. She is currently a postdoc researcher in CIMITEC, Universitat Autònoma de Barcelona, Spain. Her current research interests focus on the development of novel microwave sensors with improved performance for biosensors, dielectric characterization of solids and liquids, defect detection, industrial processes, etc.

Ferran Martín (M'04-SM'08-F'12) was born in Barakaldo (Vizcaya), Spain in 1965. He received the B.S. Degree in Physics from the Universitat Autònoma de Barcelona (UAB) in 1988 and the PhD degree in 1992. From 1994 up to 2006 he was Associate Professor in Electronics at the Departament d'Enginyeria Electrònica (Universitat Autònoma de Barcelona), and since 2007 he is Full Professor of Electronics. In recent years, he has been involved in different research activities including modelling and simulation of electron devices for high frequency applications, millimeter wave and THz generation systems, and the application of electromagnetic bandgaps to microwave and millimeter wave circuits. He is now very active in the field of metamaterials and their application to the miniaturization and optimization of microwave circuits and antennas. Other topics of interest include microwave sensors and RFID systems, with special emphasis on the development of high data capacity chipless-RFID tags. He is the head of the Microwave Engineering, Metamaterials and Antennas Group (GEMMA Group) at UAB, and director of CIMITEC, a research Center on Metamaterials supported by TECNIO (Generalitat de Catalunya). He has organized several international events related to metamaterials and related topics, including Workshops at the IEEE International Microwave Symposium (years 2005 and 2007) and European Microwave Conference (2009, 2015 and 2017), and the Fifth International Congress on Advanced Electromagnetic Materials in Microwaves and Optics (Metamaterials 2011), where he acted as Chair of the Local Organizing Committee. He has acted as Guest Editor for six Special Issues on metamaterials and sensors in five International Journals. He has authored and co-authored over 650 technical conference, letter, journal papers and book chapters, he is co-author of the book on Metamaterials entitled *Metamaterials with Negative Parameters: Theory, Design and Microwave Applications* (John Wiley & Sons Inc.), author of the book *Artificial Transmission Lines for RF and Microwave Applications* (John Wiley & Sons Inc.), co-editor of the book *Balanced Microwave Filters* (Wiley/IEEE Press), co-author of the book *Time-Domain Signature Barcodes for Chipless-RFID and Sensing Applications* (Springer) and coauthor of the book *Planar Microwave Sensors* (Wiley/IEEE Press). Ferran Martín has generated 22 PhDs, has filed several patents on metamaterials and has headed several Development Contracts. Prof. Martín is a member of the IEEE Microwave Theory and Techniques Society (IEEE MTT-S). He is reviewer of the IEEE Transactions on Microwave Theory and Techniques and IEEE Microwave and Wireless Components Letters, among many other journals, and he serves as member of the Editorial Board of IET Microwaves, Antennas and Propagation, International Journal of RF and Microwave Computer-Aided Engineering, and Sensors. He is also a member of the Technical Committees of the European Microwave Conference (EuMC) and International Congress on Advanced Electromagnetic Materials in Microwaves and Optics (Metamaterials). Among his distinctions, Ferran Martín has received the 2006 Duran Farell Prize for Technological Research, he holds the Parc de Recerca UAB – Santander Technology Transfer Chair, and he has been the recipient of three ICREA ACADEMIA Awards (calls 2008, 2013 and 2018). He is Fellow of the IEEE and Fellow of the IET.